Contents lists available at ScienceDirect

Comptes Rendus Chimie

www.sciencedirect.com

Preliminary communication/Communication

Physically activated microporous carbon from a new biomass source: Date palm petioles

Préparation de charbons actifs microporeux à partir d'une nouvelle matière première issue de la biomasse : les pétioles de palmiers dattiers

Souad Rezma [a, b, c], Marc Birot [a], Amor Hafiane [b], Hervé Deleuze [a, *]

[a] Institute of Molecular Sciences (ISM, UMR CNRS 5255), University of Bordeaux, 33400 Talence, France
[b] Laboratory of Water, Membranes and Environmental Biotechnology, CERTE, BP 273, Soliman, 8020, Tunisia
[c] Faculty of Sciences of Tunis, El-Manar University Campus, 2092, El Manar Tunis, Tunisia

ARTICLE INFO

ABSTRACT

Activated carbons were prepared from a new lignocellulosic biomass source: date palm petioles. The activation process comprise the pyrolysis to 1000 °C under nitrogen flow and then the activation at 750, 850 and 900 °C under CO_2 flow. The samples were characterized by N_2 adsorption, scanning electron microscopy and mercury porosimetry. The activated carbons exhibited a predominant microporosity with specific surface area from 225 $m^2 \cdot g^{-1}$ to 546 $m^2 \cdot g^{-1}$, and micropore volumes from 0.09 $cm^3 \cdot g^{-1}$ to 0.23 $cm^3 \cdot g^{-1}$.
© 2017 Académie des sciences. Published by Elsevier Masson SAS. This is an open access article under the CC BY-NC-ND license (http://creativecommons.org/licenses/by-nc-nd/4.0/).

RÉSUMÉ

Des charbons actifs ont été préparés à partir d'une nouvelle matière première issue de la biomasse : les pétioles de palmiers dattiers. Le processus d'activation comporte deux étapes. Dans un premier temps, la pyrolyse des échantillons a été conduite jusqu'à une température de 1000 °C sous flux d'azote. Les monolithes carbonés obtenus ont ensuite été activés physiquement à 750°, 850° et 900° C sous flux de CO_2. Tous les échantillons ont été caractérisés par adsorption d'azote, microscopie électronique à balayage et porosimétrie au mercure. Les charbons actifs présentent une microporosité importante, avec des surfaces spécifiques allant de 225 $m^2 \cdot g^{-1}$ à 546 $m^2 \cdot g^{-1}$, et des volumes microporeux variant entre 0,09 $cm^3 \cdot g^{-1}$ et 0,23 $cm^3 \cdot g^{-1}$.
© 2017 Académie des sciences. Published by Elsevier Masson SAS. This is an open access article under the CC BY-NC-ND license (http://creativecommons.org/licenses/by-nc-nd/4.0/).

1. Introduction

Activated carbon is a versatile material with large surface area, adequate pore size distribution, good thermal

* Corresponding author.
 E-mail address: h.deleuze@ism.u-bordeaux1.fr (H. Deleuze).

stability, and various functional groups at the surface [1]. In the last decade, activated carbon received considerable attention due to its attractive characteristics that promote powerful utilization for a variety of applications such as adsorption [2], energy storage [3], electrochemical application (super capacitor) [4] and catalysis [5]. The preparation of activated carbon from cheap and readily available agricultural by-products (date stone [6], rice hulls [7], olive stone [8], grape seeds [9], cassava peel [10], etc.) has lured attention from economic and environmental aspects. Activated carbon can be prepared from carbonaceous precursors by different activation methods [11]. Basically they can be activated by chemical and physical methods. Typically, when performed by chemical methods, the raw material is mixed with active agents such as (H_3PO_4 [12] $ZnCl_2$ [13] and KOH [14]) followed by heat treatment at temperatures between 400 °C and 900 °C, carbonization and activation being performed simultaneously. On the other hand, the physical procedure implies the pyrolysis of the raw material under N_2 at a higher temperature (800 −1000 °C), followed by activation under gas flow like CO_2, water vapor or a mixture of them.

The palm tree, a plant cultivated in Tunisia, is rich in by-products but it is currently poorly valued. Interestingly, the date stone, leaves, wood and petioles may serve as precursors for the preparation of activated carbon. In the present study, we focused on the preparation of activated carbons from date palm petioles using physical activation with CO_2 at different temperatures. The materials obtained were characterized by different techniques such as nitrogen sorption, scanning electron microscopy and thermal analysis to gain insights on the surface properties.

2. Experimental procedures

2.1. Raw materials and treatment

Palm wastes, namely date palm petioles (Fig. 1), were obtained from a date palm oasis in Gabès, Tunisia. Petioles were washed with distilled water to remove dust and other hydrophilic impurities, and then dried at room temperature. After being dried, they were cut into small pieces.

Fig. 1. Visual aspect of a raw date palm petiole.

2.2. Activated carbon preparation

Pyrolysis and physical activation were carried out in a horizontal tube furnace. In a typical experiment, a palm petiole sample (30 g) was placed in a furnace under N_2 flow (100 mL·min^{-1}). The thermal program was as follows: heating from room temperature to 1000 °C at a 1 °C·min^{-1} rate including a first plateau at 300 °C for 4 h, then a second one at 700 °C for 2 h and a final maintenance at 1000 °C for 2 h. The cooling process was not controlled and therefore directed by the oven inertia.

The obtained chars were then activated under CO_2 flow (100 mL·min^{-1}) at different temperatures: 750 °C, 850 °C and 950 °C for 30 min at a heating rate of 5 °C·min^{-1}.

The different samples are referred as raw date palm petiole (**PP**), carbonized palm petiole (**CPP**) and activated palm petiole (**APP**). Samples nomenclature also includes the activation temperature; for example **APP750** refers to the carbonized palm petiole activated at 750 °C.

2.3. Samples characterizations

2.3.1. Yield and burn-off

The pyrolysis yield was defined as: % Yield = $100 \times \left[m_{(\text{after pyrolysis})} / m_{(\text{before pyrolysis})} \right]$. Burn-off is defined as the weight difference between the precursor biomass and the activated carbon. The following relationship was used: % burn-off = $100 - [(m_{\text{after activation}}) / m_{\text{precursor}}) \times 100]$.

2.3.2. Nitrogen sorption analysis

The specific surface area was determined by nitrogen sorption measurements in a Micromeritics ASAP 2010 analyzer. The total pore volume, V_{total}, was obtained from the amount of gas adsorbed at a relative pressure p/p_0 of 0.99. The collected data were subjected to the Brunauer, Emmett, and Teller (BET) treatment [15]. The microporous volume (V_{micro}) and the microporous specific surface area (S_{micro}) were obtained by the application of the t-plot method [16] to the nitrogen adsorption data. The pore size distribution of the materials was assessed by the density functional theory (DFT) [17].

2.3.3. Thermogravimetric analysis (TGA)

The weight loss studies of the materials were performed in a Netzsch STA 409 thermobalance under high purity argon flow (60 mL·min^{-1}). The TGA data were obtained at a heating rate of 5 °C·min^{-1} and the temperature ranged from 30 to 1000 °C.

2.3.4. Microscopy analysis

The morphologies of **PP**, **CPP** and **APP** samples were observed by scanning electron microscopy (SEM) using a Hitachi TM-1000 microscope. To run the analysis, pieces of samples (sections of about 0.5 cm^2) were cut from the corresponding monoliths and then mounted on a carbon tab, which ensured a good conductivity. A thin layer of gold-palladium was sputtered on the sample fragment prior to analysis. Micrographs were taken at several different magnifications between ×500 and ×10,000.

2.3.5. Skeletal density

The skeletal density (ρ_s) of the materials was determined using a Micromeritics Accupyc II 1340 helium pycnometer.

2.3.6. Elemental analysis

The C, H, N, S and O elemental analyses were carried out at ISM (CESAMO) using a Thermo Fisher Flash 2000 analyzer ensuring a precision of ±0.3%.

2.3.7. Mercury intrusion porosimetry analysis

The experimental open porosity Φ_{exp}, pore size distribution and skeletal density of each sample were determined by mercury intrusion porosimetry in a Micromeritics Autopore IV 9500 porosimeter with the following parameters: contact angle = 130°, mercury surface tension = 485 mN·m^{-1}, maximum intrusion pressure = 124 MPa.

2.3.8. Conductivity measurement

Conductivity measurements were obtained through the four-point van der Paw technique, using direct current. A 2000 Keithley multimeter (Keithley Instruments Inc., Solon, OH, USA) was used for conductivity (resistance) measurements while employing a Keithley 2220 precision current source apparatus. The samples were chiseled using a diamond saw. Disks bearing radius of 2.5 mm and a 3 mm thickness were generated. For the sake of standard deviation, three disks of each sample were prepared.

2.3.9. Raman spectroscopy

Raman spectra were recorded at 297 K on a Xplora confocal micro-Raman spectrometer (Horiba Jobin-Yvon), in back scattering geometry at 2.33 eV laser energy (532 nm) with a typical spectral resolution of 1.7 cm^{-1} (lens ×50). We managed to irradiate below an incident power of 1 mW in order to avoid sample damaging.

3. Results and discussion

3.1. Characterization of raw palm petiole (PP)

The visual aspect of the raw palm petiole (PP) sample is shown in Fig. 2a.

The skeletal density of PP was estimated by helium pycnometry at $\rho_s = 1.54 \pm 0.08$ g·cm^{-3}, a value comparable to that of other lignocellulosic materials [18].

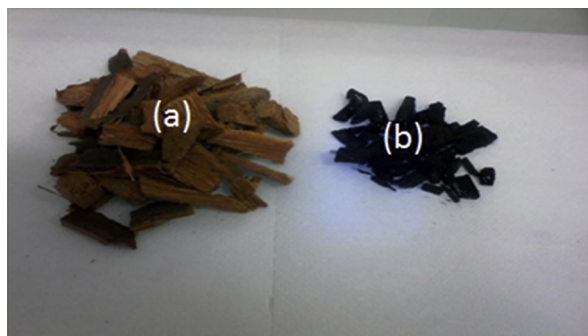**Fig. 2.** Visual aspect of **PP** (a) and **CPP** (b) samples.
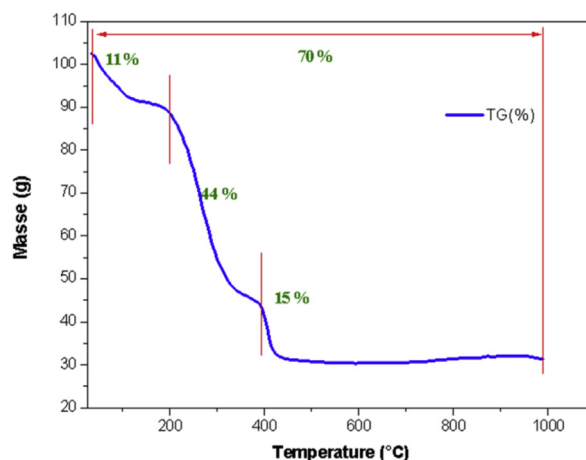

Fig. 3. Thermogravimetry plot of raw palm petiole **PP**.

The TG analysis of raw palm petiole **PP** is represented in Fig. 3. The weight loss occurred in a temperature range of 30−1000 °C. Three stages of evolution were observed during the pyrolysis of the sample: dehydration, decomposition of the material and carbonization. The TG curve shows a first weight loss (11%) until (about) 180 °C due to loss of water. The second weight loss (44%), occurring between 180 °C and 370 °C, corresponds to the decomposition of cellulose and also the elimination of volatile matters and tars. The third stage arising between 370 °C and 705 °C, where up to 15% of weight loss was observed, is due to the decomposition of lignin [19]. Above 705 °C, the weight of the sample became constant indicating that the basic structure of the char has been formed. The total weight loss was about 71%.

3.2. Characterization of carbonized (CPP) and activated (APP) materials

3.2.1. Yield and burn-off determination

The yield of the pyrolysis sample (**PP**) and the burn-off of activated samples (**APP750** and **APP850**) are reported in Table 1.

Table 1
Yield and burn-off.

Sample	Yield (% w)	Burn-off (% w)
CPP	31.6	
APP750		42.3
APP850		78.6
APP950		58.6

Table 2
Elemental analyses of the materials.

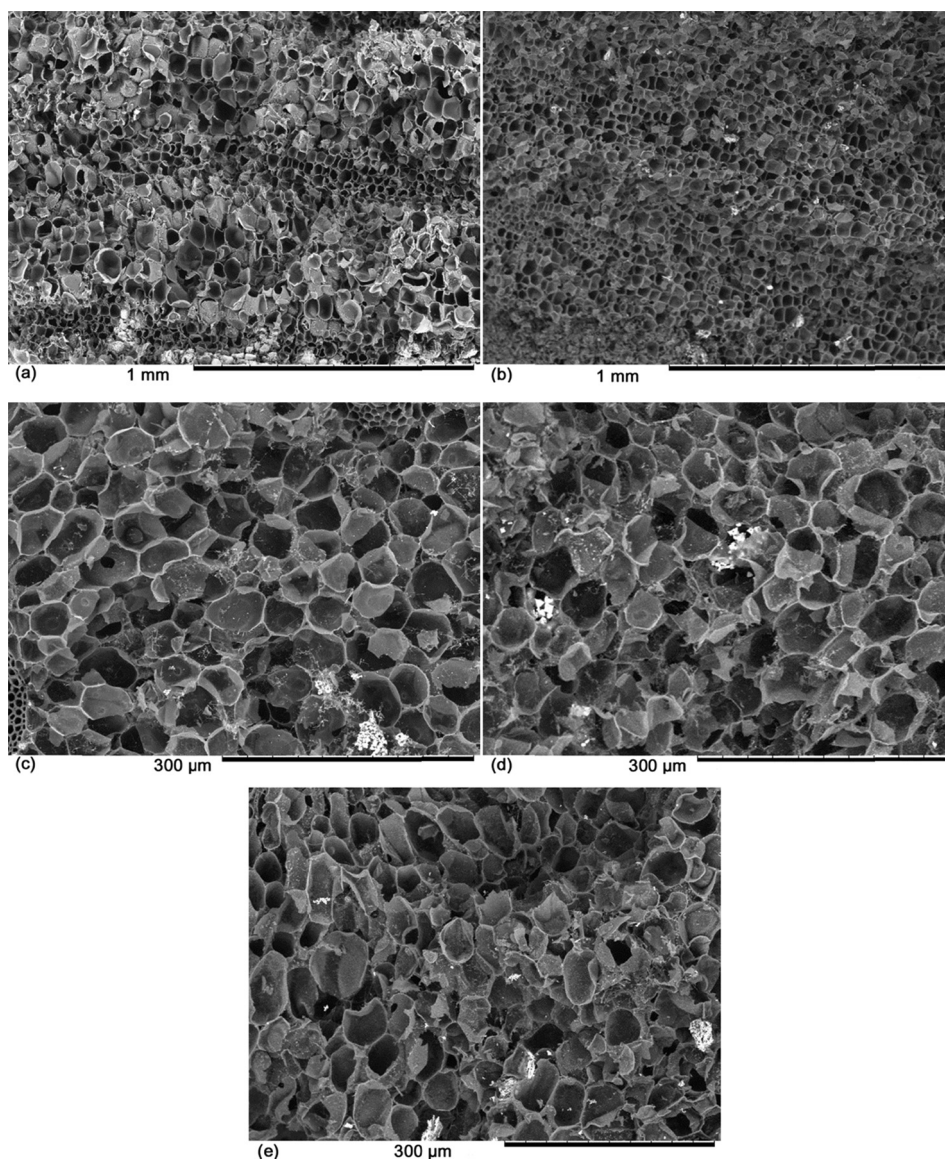| Sample	C (% w)	H (% w)	N (% w)	O (% w)	S (% w)	C/H	C/O
PP	36.16	4.63	0.34	41.87	2.38	7.80	0.86
CPP	59.27	1.60	0.62	16.76	2.79	37.04	3.53
APP750	62.94	1.01	0.56	12.27	4.18	62.31	5.12
APP850	63.42	1.06	0.75	12.59	4.24	59.83	5.04
APP950	53.67	0.96	0.26	13.39	5.83	55.90	4.01

Fig. 4. SEM micrographs of **PP** (a), **CPP** (b), **APP750** (c), **APP850** (d), **APP950** (e).

The increase of the burn-off with activation temperature is an indication of the corresponding increase of mesoporosity and microporosity volumes of the different samples.

3.2.2. Elemental analysis

The elemental analyses of the different samples are reported in Table 2. The PP sample contains essentially C and O with less N. The presence of S may be due to the effects of industrial pollution from the sulfuric acid factories close to the oasis. Data reported indicate a strong increase in C/H and C/O mass ratios during the pyrolysis step, suggesting that a polymerization process occurs, hence increasing the aromatic degree of the material. The pyrolysis and activation lead to an increase in the carbon percentage in contrast to hydrogen and oxygen contents. The sulfur contents remain significant. The pyrolysis stage under neutral atmosphere allows obtaining a carbonaceous product by the volatilization of hydrogen, oxygen and nitrogen traces [20].

3.2.3. Microscopy analysis

The samples **PP**, **CPP**, **APP750**, **APP850** and **APP950** are shown in Fig. 4. Raw palm petiole **PP** (Fig. 4a) has a natural porous structure that appears to be maintained after pyrolysis as observed in Fig. 4b. After activation, samples **APP750** (Fig. 4c), **APP850** (Fig. 4d), and **APP950** (Fig. 4e) have a similar porous morphology. This indicates that the range of temperature used in this study did not produce significant differences in porous morphology [21].
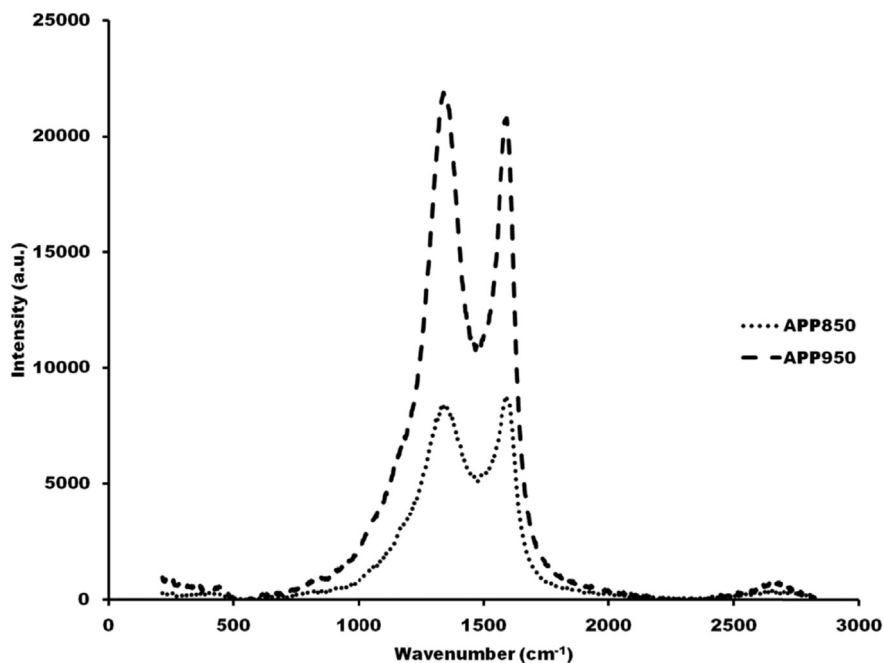
Fig. 5. Raman spectra of carbonaceous samples pyrolysed at various temperatures. ($\cdots$) **APP850**, (---) **APP950**.

3.2.4. Raman spectroscopy

The Raman spectra of **APP850** and **APP950** are reported in Fig. 5.

From the Raman spectra, two main bands can be seen in the region of 1000−1750 cm^{-1}. The band centered at 1337 cm^{-1} that corresponds to vibrations of tetrahedral (sp^3) carbon atoms, known as D-band, and another band centered at 1584 cm^{-1} that corresponds to two dimensional in-plane motion of strongly coupled sp^2 carbons (E$_{2g}$ symmetry) in the honeycomb network of the graphite lattice [22], labeled thus G-band. It can be observed that the intensity of the disorder parameter $I_D/(I_D + I_G)$ decreases from 51.2% for **APP850** to 49.4% for **APP950**. Overall, this scenario shows that date palm petioles used in this work as a carbonaceous source are not favoring the enhancement of graphitic crystalline form over amorphous sp^3 one when increasing the temperature from 850 °C up to 900 °C.
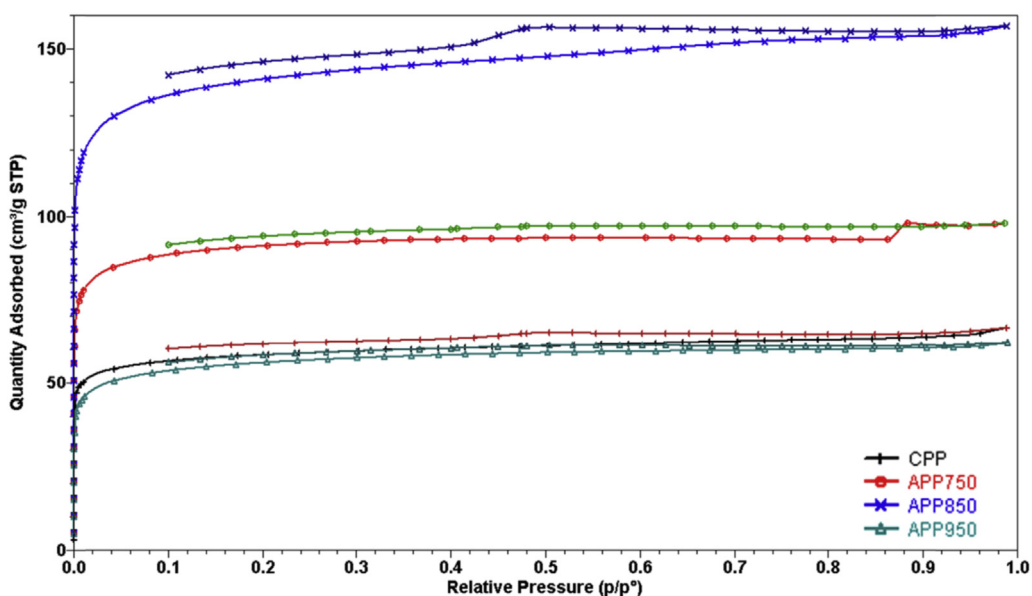

Fig. 6. N$_2$ sorption isotherms of pyrolyzed (**CPP**) and activated (**APP750**, **APP850**, **APP950**) samples.

Table 3
Nitrogen sorption results of pyrolyzed and activated carbons.

Sample	BET method		t-plot method	
	S_{BET} (m^2·g^{-1})	V_{total} (cm^3·g^{-1})	S_{micro} (m^2·g^{-1})	V_{micro} (cm^3·g^{-1})
CPP	225	0.10	219	0.09
APP750	353	0.15	351	0.14
APP850	546	0.24	540	0.23
APP950	214	0.10	210	0.09

3.2.5. Porous volumes and specific surface area determination

The experimental open porosity Φ_{exp} (%) of the different samples was determined by mercury intrusion porosimetry. The obtained values are**:** 87%; 90%; 90% and 91% for **CPP**, **APP750**, **APP850** and **APP950**, respectively. We noted a slight increase in the experimental porosity after activation. The maximum porosity was obtained for the temperature 950 °C. The skeletal density of the carbonized material **CPP** was found to be $\rho_s = 1.76 \pm 0.08$ g·cm^{-3}, and those of the activated carbons $\rho_s = 1.88 \pm 0.07$ g·cm^{-3}, for all samples. These values are consistent with that of amorphous carbons [23]. The average macropore diameters of the activated samples are in the range of 50–75 μm, similar with those of the native palm petiole. The porous structure of the palm petiole appears to be maintained after pyrolysis and activation.

The nitrogen adsorption/desorption isotherms at 77 K of samples **CPP**, **APP750**, **APP850** and **APP950** are reported in Fig. 6. The isotherm profiles are type I. As classified by IUPAC, type-I isotherms are obtained with microporous materials [24]. As can be seen from Fig. 4, for all samples **CPP**, **APP750**, **APP850** and **APP950**, the main uptake occurs at low relative pressure (less than 0.1) showing the formation of microporous materials. The hysteresis loops owing to capillary condensation in mesopores are not very distinct, indicating that the samples possess only a limited mesoporosity.

Then, different pore volumes and specific surface area were determined from the data collected from the isotherms using specific methods (Table 2). The specific surface area S_{BET} [15] of some samples activated are higher than those of non activated palm petiole ($S_{BET} = 353$ and 546 m^2·g^{-1} for **APP750** and APP850, respectively). In the case of the sample activated at 950 °C (**APP950**), the specific surface area S_{BET} decreased after activation and achieved a value comparable to that of non activated materials ($S_{BET} = 214$ and 225 m^2·g^{-1} for **APP950** and **CPP**, respectively). This behavior is also observed for the total pore volume which increased from 0.15 to 0.24 cm^3·g^{-1} as the activation temperature was raised from 750 °C to 850 °C and then decreased when the activation temperature reached 950 °C (0.09 cm^3·g^{-1}). This may be attributed to the decomposition of the material at high temperature under an oxidizing atmosphere. The t-plot method allows the determination of pore volumes and specific surface areas of micropores (pores of diameter less than 2 nm) [16]. As expected from the isotherms shape (Fig. 5), the entire sample series exhibits high micropore specific surface area values S_{micro} (Table 3). The micropore volume and specific surface area for **APP850** are higher than for the other samples. In view of the results obtained, in this study 850 °C was regarded as the optimum activation temperature.

The pore size distribution of the pyrolyzed and activated samples have been obtained by DFT calculations [17], considering slit-shaped pores. As observed in Fig. 7, all the samples show a pore size range of 0.6–1.2 nm with multiple peaks and a predominant maximum ≤0.7 nm, indicating the presence of micropores, while the mesopore contribution is negligible which is consistent with the previous observations.

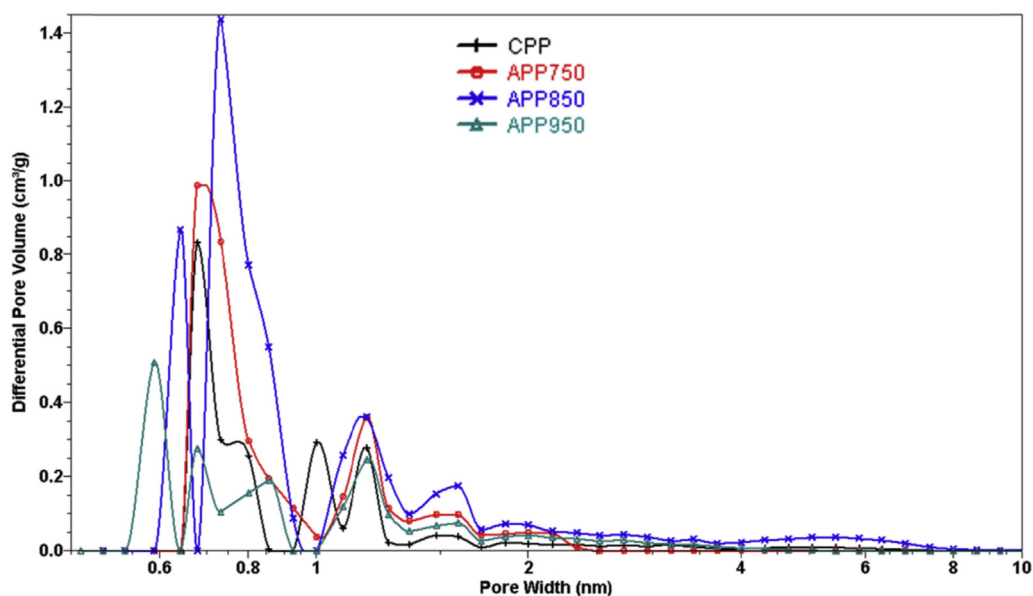**Fig. 7.** DFT pore size distribution of the pyrolyzed (**CPP**) and activated (**APP**) carbons.

3.2.6. Electrical properties

Electronic transport measurements have been performed on the date petiole activated at 850 °C (**APP850**). The electric conductivity is as follows: $\sigma = 12$ S·m^{-1} $\pm$ 0.5 S·m^{-1} This conductivity value is lower than those already reported for macroporous carbons prepared from lignocellulosic raw sources such as kraft black liquor [18].

4. Conclusions

Preparation of activated carbons from a new source of raw material: date palm petioles, proved to be very effective. This work shows that date palm petioles can be used as a precursor to produce activated carbons by pyrolysis followed by physical activation with CO_2. Porosity analysis showed that a temperature of activation 850 °C during 30 min under CO_2 flow can be regarded as optimum treatment. The activated carbons thus obtained are essentially microporous, with a BET specific surface area of 546 m^2·g^{-1}.

References

[1] J.N. Sahu, J. Acharya, B.C. Meikap, Bioresour. Technol. 101 (2010) 1974–1982.
[2] Y. Sun, H. Li, G. Li, B. Gao, Q. Yue, X. Li, Bioresour. Technol. 217 (2016) 239–244.
[3] T. Ramesh, N. Rajalakshmi, K.S. Dhathathreyan, J. Energy Storage 4 (2015) 89–95.
[4] A.M. Abioye, F.N. Ani, Renew. Sustain. Energy Rev. 52 (2015) 1282–1293.
[5] B. Meryemoglu, S. Irmak, A. Hasan-oglu, Fuel Process Technol. 151 (2016) 59–63.
[6] M.L. Sekirifa, M. Hadj-Mahammed, S. Pallier, L. Baameur, D. Richard, A.H. Al-Dujaili, J. Anal. Appl. Pyrolysis 99 (2013) 155–160.
[7] L. Muniandy, F. Adam, A. Rahman Mohamed, Eng-Poh Ng, Microporous Mesoporous Mater. 197 (2014) 316–323.
[8] I. Ghouma, M. Jeguirim, S. Dorge, L. Limousy, C. Matei Ghimbeu, A. Ouederni, C. R. Chimie 18 (2015) 63–74.
[9] I. Okman, S. Karagöz, T. Tay, M. Erdem, Appl. Surf. Sci. 293 (2014) 138–142.
[10] Y. Sudaryanto, S.B. Hartono, W. Irawaty, H. Hindarso, S. Ismadji, Bioresour. Technol. 97 (2006) 734–743.
[11] N.A. Rashidi, S. Yusup, Chem. Eng. J. 314 (2017) 270–290.
[12] X. Duana, C. Srinivasakannand, X. Wange, F. Wanga, X. Liu, J. Taiwan Inst. Chem. Eng. 70 (2017) 374–381.
[13] E. Altintig, S. Kirkil, J. Taiwan Inst. Chem. Eng. 63 (2016) 180–188.
[14] N.T. Abdel-Ghani, G.A. El-Chaghaby, M.H. El-Gammal, El-Shaimaa A. Rawash, New Carbon Mater. 31 (2016) 492–500.
[15] S. Brunauer, P.H. Emmett, E.J. Teller, J. Am. Chem. Soc. 60 (1938) 309–319.
[16] B.C. Lippens, J.H. de Boer, J. Catal. 4 (1965) 319–323.
[17] P. Tarazona, Surf. Sci. 331–333 (1995) 989–994.
[18] A. Foulet, M. Birot, G. Sonnemann, H. Deleuze, React. Funct. Polym. 90 (2015) 15–20.
[19] J.J. Kong, Q.Y. Yue, P. Zhao, B.Y. Gao, Q. Li, Y. Wang, H.H. Ngo, W.S. Guo, Fuel Process Technol. 140 (2015) 67–75.
[20] F. Kifani-Sahban, L. Belkbir, A. Zoulalian, Thermochim. Acta 284 (1996) 341–349.
[21] K.G. Mansaray, A.E. Ghaly, Energy Sources 21 (1999) 773–784.
[22] F. Tuinstra, J.L. Koening, J. Chem. Phys. 53 (1970) 11626–11630.
[23] W.M. Haynes, D.R. Lide, CRC Handbook of Chemistry and Physics, 91st ed., CRC Press, New York, 2010, pp. 4–8.
[24] K.S.W. Sing, D.H. Everett, R.A.W. Haul, L. Moscou, R.A. Pierotti, J. Rouquerol, T. Siemieniewska, Pure Appl. Chem. 57 (1985) 603–619.